UNIVERSIDAD SAN FRANCISCO DE QUITO

Colegio de Ciencias e Ingeniería

Residual Stress in High Velocity Impact Coatings: Modeling Approach

Juan Felipe Oviedo Perhavec

Alfredo Valarezo, Ph.D., Director de Tesis

Tesis de grado presentada como requisito
para la obtención del Título de Ingeniero Mecánico

Quito, mayo de 2014

UNIVERSIDAD SAN FRANCISCO DE QUITO

Colegio de Ciencias e Ingeniería

HOJA DE APROBACIÓN DE TESIS

Residual Stress in High Velocity Impact Coatings: Modeling Approach

Juan Felipe Oviedo Perhavec

Alfredo Valarezo, Ph.D.
Director de Tesis _____

Lorena Bejarano, Ph.D.
Miembro del Comité de Tesis _____

Patricio Chiriboga, Ph.D.
Miembro del Comité de Tesis _____

Alfredo Valarezo, Ph.D.
Coordinador de Ingeniería Mecánica_____

Ximena M. Córdova, Ph.D.
Decana de Escuela de Ingeniería _____
Colegio de Ciencias e Ingeniería

Quito, mayo de 2014

© DERECHOS DE AUTOR

Por medio del presente documento certifico que he leído la Política de Propiedad Intelectual de la Universidad San Francisco de Quito y estoy de acuerdo con su contenido, por lo que los derechos de propiedad intelectual del presente trabajo de investigación quedan sujetos a lo dispuesto en la Política.

Asimismo, autorizo a la USFQ para que realice la digitalización y publicación de este trabajo de investigación en el repositorio virtual, de conformidad a lo dispuesto en el Art. 144 de la Ley Orgánica de Educación Superior.

Firma: _____

Nombre: Juan Felipe Oviedo Perhavec

C. I.: 1718615840

Lugar: Quito, mayo de 2014.

DEDICATORIA

A mis profesores en la USFQ, por la generosidad y el desinterés al compartir su conocimiento, su tiempo y su experiencia mucho más allá de las exigencias de su trabajo.

A mis amigos, dentro y fuera de la USFQ, por su aliento y compañía constante en los momentos de felicidad y tristeza, fracaso y triunfo.

A Camila, por el amor, la felicidad y la cercanía.

A mi padre Edmundo, por el amor, la lucidez y el sacrificio.

A mi madre Adriana, por el amor, la constancia y la entrega.

A mi hermana Gabriela, por el amor, la compañía y la risa.

A Dios.

AGRADECIMIENTOS

"All exact science is dominated by the idea of approximation. When a man tells you that he knows the exact truth about everything, you are safe in inferring that he is an inexact man"

Bertrand Russell

El autor desea expresar su sincera gratitud a agradecer a su Director de Tesis, Prof. Alfredo Valarezo, por su extensa paciencia, constante motivación, generoso conocimiento y compromiso durante el proceso de investigación y redacción de este trabajo.

A su vez, el autor agradece a los Miembros de Comité de Tesis, Prof. Patricio Chiriboga y Prof. Lorena Bejarano, por su importante y oportuno aporte en la revisión y crítica del manuscrito final.

Es necesario destacar los importantes aportes de Prof. Sanjay Sampath de Stony Brook University, EE.UU. y la valiosa amistad e interés de Anssi Laukkanen y Tatu Pinomaa de VTT, Finlandia.

Es apropiado destacar el apoyo, buena voluntad y compañía de mis compañeros y amigos durante mis años universitarios Paola, Alejandro, Marcos, Hugo, Luis, Daniel, Esteban, Alfonso y muchos otros.

Por último, pero no menos importante, el autor desea agradecer a toda su familia, en especial a sus padres, Edmundo y Adriana, y su hermana, Gabriela, por su apoyo constante, su ejemplo indeleble y su amor.

RESUMEN

Los recubrimientos de alta velocidad de impacto son producidos mediante técnicas tales como rociado en frío, rociado cinético, rociado caliente, HVOF, rociado de plasma supersónico, etc. Todos estos procesos tienen en común el impacto de partículas a altas velocidades que produce *peening* en la superficie e induce esfuerzo residual compresivo en dirección planar hacia el recubrimiento. Si el proceso involucra un ingreso de calor significativo, enfriamiento súbito de *splats* y descompensación térmica entre recubrimiento y sustrato, un esfuerzo residual térmico es sumado al esfuerzo provocado por el *peening* para definir el estado de esfuerzo final del sistema.

En el presente trabajo se estudia variables físicas como velocidad y temperatura de partícula, masa de partícula, morfología de partícula, masa de partícula y temperatura local de deposición del sustrato con el fin de observar su efecto sobre el esfuerzo residual, y definir su posible manipulación para el diseño de recubrimientos con esfuerzo residual promedio adecuado. Por ejemplo, para aumentar el efecto de *peening,* las partículas pueden ser proyectadas a mayor velocidad mientras se mantiene la temperatura local de deposición del sustrato baja. Modelar el impacto y enfriamiento de partículas durante la deposición del recubrimiento permite realizar una selección de parámetros clave a través de un análisis de sensibilidad. Un mapa de contorno es producido para selección de parámetros en base a simulación de impacto de partícula (empleando FEA Explicit) y la subsecuente simulación de formación de recubrimiento capa-por-capa (empleando FEA Implicit) mediante el código ABAQUS. El modelo Johnson-Cook para alta deformación, tasa de deformación y temperatura es usado como la ecuación constitutiva para el estudio del impacto y rápido enfriamiento de partículas en este modelo.

ABSTRACT

High velocity impact coatings are produced by techniques such as cold spray, kinetic spray, warm spray, HVOF, supersonic plasma spraying, etc. All these processes have in common the impact of particles at high velocities that produce peening of the surface and induce compressive residual stresses in the in-plane orientation in the coating. If the process involves a significant heat input, quenching of splats and thermal mismatch between coating and substrate, it would add residual stress to the peening to define the final stress state.

Physical variables, including: particle temperature and velocity, particle mass, particle morphology, and local deposition temperature are studied to observe their effect on residual stresses, and define their possible manipulation to design coatings of desired average residual stress. For instance, to increase the peening effect, particles can be projected faster while keeping the local deposition temperature low. Modeling the impact of particles allows to resolve for key parameter selection via a sensitivity analysis. A contour map is produced for parameter selection based on the modeling of particle impact (via a FEA Explicit Model) and the subsequent layer-by-layer coating formation (via a FEA Implicit Model) employing ABAQUS code. The Johnson-Cook model for high strain, strain rate and temperature is used as the constitutive equation for the study of impact and rapid cooling.

CONTENTS

Resumen **7**

Abstract **8**

INTRODUCTION **12**

MATERIALS AND METHODS **17**
Finite element (FE) model **17**
Explicit particle impact analysis. 19
Impact parametric analysis 24
Implicit layer deposition analysis. 28

RESULTS **32**
Individual particle effects on the stress profile **32**
Effects of particle state: velocity and temperature. 33
Effects of particle mass and morphology. 35
Effects of substrate condition: local deposition temperature. 38
Through thickness residual stress profiles: response to local deposition temperature. **39**

DISCUSSION **42**
Single particle impact **42**
Through thickness residual stress profiles **45**
Correlation between parameters **49**

CONCLUSIONS **54**

REFERENCES **55**

APPENDIX A: ABAQUS MODEL CODE **60**

TABLES

Table 1: Thermomechanical properties and JC model parameters for SS316. 23

FIGURES

Figure 1: Flowchart of the hybrid explicit-implicit FE methodology of the model. 19

Figure 2: Axisymmetric single particle impact model 21

Figure 3: Stress as function of plastic strain for **a)** different temperatures and constant strain rate and **b)** different strain rates and constant temperature calculated through SS316 JC model. 24

Figure 4: Axisymmetric particle shapes of equal mass and its calculated area moment of inertia with respect to the vertical axis. 27

Figure 5: Cooling curves of a 10 um diameter splat for several overall substrate temperatures. 28

Figure 6: Axisymmetric implicit layer deposition model for SS316. 31

Figure 7: Splat shapes and residual in-plane stress field (in Pa) after impact for two particles whose initial temperatures are 800 [K] and 1600 [K]. 32

Figure 8: Residual in-plane stress as a function of substrate depth for different particle velocities. 34

Figure 9: Residual in-plane stress as a function of substrate depth for different particle temperatures. 35

Figure 10: Residual in-plane stress as a function of substrate depth for different spherical particle diameters 37

Figure 11: Residual in-plane stress as a function of substrate depth for different area moments of inertia with respect to vertical axis 38

Figure 12: Residual in-plane stress as a function of substrate depth for different local deposition temperatures 39

Figure 13: Quenching and thermal in-plane stress (a), peening in-plane stress (b) and total residual in-plane stress (c) as a function of substrate depth for different local deposition temperatures 41

Figure 14: Average in-plane residual stress in coating as a function of particle velocity for different local deposition temperatures. 50

Figure 15: Average in-plane residual stress in coating as a function of local deposition temperatures for different particle velocities. 51

Figure 16: Contour map of average residual stress in coating as a function of local deposition temperature and particle velocity. 52

INTRODUCTION

In general, high velocity (HV) spraying techniques are the preferred manufacturing processes for thick metal/alloy and hard cermet coatings. HV impact coating technologies may include: cold spraying, kinetic spraying, warm spraying, supersonic plasma spraying, detonation spraying, and high velocity oxy-fuel (HVOF) spraying. HV impact technologies are capable of producing dense structures at a high deposition rate relative to other surface technologies. However, some limitations of the process arise especially due to residual stresses. Some of these issues are limited coating thickness, premature debonding, cracking, etc. In all these techniques, the effects of particle impact and temperature gradients significantly contribute to the final stress state of the coatings-substrate system.

Residual stresses are inherently present in HV impact coatings as in any other manufacturing process where expansion mismatch of materials, peening effects or temperature gradients have influence. As supported by numerous experimental studies (Clyne & Gill, 1996; X. Zhang, Watanabe, & Kuroda, 2013), fatigue life and adhesion strength are highly dependent of the final residual stress state of the coating. Coatings subjected to tensile stress after deposition tend to have minor fatigue lives compared to those subjected to compression (McGrann et al., 1998). Adhesion strength is also negatively affected when severe shifts in the stress profile in coating/substrate interface occur. This affectation is caused by increase of the energy release rate at the interface, and it significantly enhances the debonding probability (Godoy, Souza, Lima, & Batista, 2002; Howard, Tsui, & Clyne, 1994). The final residual stress in HV impact coatings is a combination of

stresses generated during peening, quenching and cooling processes of molten or solid particles, determined by physical variables such as particle state, particle morphology or substrate temperature. Process and hardware parameters, such as feedstock, torch gas flow or feed rate, directly determine physical variables. Thus, a strategic process design before deposition has an important effect in tailoring and optimizing the final residual stress distribution and, in consequence, the coating quality and reliability. Simulation, parameterization and sensitivity analysis generate adequate frameworks for process design (H Assadi et al., 2011; Bemporad, Sebastiani, Casadei, & Carassiti, 2007).

While the effect of hardware variables on residual stress is well known for some specific thermal spraying processes, materials, conditions and guns, the direct influence of physical parameters is not extensively covered in literature. The objective of this work is to employ a modeling approach to predict the influence of physical parameters on residual stress and contribute with a more general framework for process design in HV impact technologies. Residual stress prediction of thermal spray coatings can be accomplished either through simple analytical models, with several limitations to account for peening stress and dynamical phenomena, or by complex and time consuming numerical methods. Analytical methods consist in force and momentum balances due to the misfit strain produced during quenching and cooling of molten material over a substrate (Tsui & Clyne, 1997; X. Zhang et al., 2013). Current analytical models are useful to predict thermally-induced stresses during an idealized static deposition process for varying material properties and dimensional conditions, but not peening. In addition, finite element (FE) models have been developed to address layer growth

and residual stress evolution under a more complex spectrum of conditions such as graded ceramic-metal interfaces (Williamson, Rabin, & Drake, 1993), multilayer coatings (Toparli, Sen, Culha, & Celik, 2007; X. C. Zhang, Xu, Wang, Jiang, & Wu, 2006), as-sprayed residual stress prediction (Ng & Gan, 2005), complex cooling conditions (Wenzelburger, Escribano, & Gadow, 2004) or specific heat source displacements (Buchmann, Gadow, & Tabellion, 2000). Both analytical and numerical methodologies have been very useful to predict stress profiles in surface technologies in which thermal interactions are determinant and impact velocities are relatively low, such as plasma spraying.

However, all these models do not account for the peening stresses generated during the non-linear and dynamical particle impact event. Residual stresses in HV impact coatings are highly dependent of the impact event and its conditions. In this case, numerical models based on explicit FE analysis, considering elastic-plastic or strain rate dependent material properties, are useful. Single particle impact has been simulated extensively employing these FE methodologies, especially for cold spraying and shot-peening processes (Hamid Assadi, Gärtner, Stoltenhoff, & Kreye, 2003; Frija, Hassine, Fathallah, Bouraoui, & Dogui, 2006; Yokoyama et al., 2006). The predicted deformation fields and particle shapes have shown to be highly coherent with appropriate coating micrographs (Li, Zhang, Li, & Liao, 2009). Single particle impact simulations are often employed to study the dynamics of impact and infer specific interactions and parameters, for instance, determination of critical velocity for particle bonding (Schmidt, Gärtner, Assadi, & Kreye, 2006), interaction with films or non-ideal interfaces (Thornton & Yin, 1991; Zouari & Touratier, 2002), behavior of molten splats (Zirari, Abdellah El-

Hadj, & Bacha, 2010) and multiple and repetitive impacts (Meguid, Shagal, & Stranart, 2002). Regarding residual stress prediction, the work of (Meguid, Shagal, & Stranart, 1999) for shot-peening found that the highest compressive magnitude after impinging is aligned with the particle central axis. In addition, it identified that particle shape and velocity are directly related to the shape and depth of the substrate plastically deformed zone upon impact.

Finally, the prediction of overall peening stress in coatings has been achieved with multiple particle deposition models through several FE approaches like hybrid implicit-explicit FE analysis (Bansal, Shipway, & Leen, 2007), inclusion of computer fluid dynamics (CFD) for considering fluid/structure interactions and coating growth (Phan, Masood, Jahedi, & Zahiri, 2010) or stochastic modeling conjugated with microstructure information and Object Oriented Finite Elements (OOF) (Ghafouri-Azar, Mostaghimi, & Chandra, 2006). For the current work, a generic hybrid implicit – explicit FE model is developed based on the methodology employed by (Bansal et al., 2007). Single particle results are extended to a layer-by-layer coating growth simulation. Residual stress profiles and average residual stresses in coating are calculated from a set of physical parameters in the HV processing range. This set of physical parameters includes particle velocity, temperature, mass and morphology, and substrate local deposition temperatures. The effect of parametric variation on residual stress is quantified. Then, these results are related to experimental evidence from literature, and physical parameters are associated to specific hardware variables. Finally, an optimal set of parameters is identified in order to increase quality and performance for the specific simulated coating material.

MATERIALS AND METHODS

Finite element (FE) model

The final residual stress profile in high velocity impact coatings is the consequence of several dynamic processes. A peening stress profile appears due to the impact of individual particles that produce plastic deformation (either the ones that stick as wells as the ones that bounce back). Quenching stress is developed by solidification and cooling of individual splats. Subsequently, thermal stresses are induced during the cooling down of coated material to ambient temperature due to the thermal expansion mismatch. The subsequent deposition of layers of material and the balance of forces and moments through the thickness determine a profile of residual stresses. The resulting stress distribution of the coated specimen is significantly dependent of the reiterative effect of all the phenomena occurring during coating formation.

In order to model this complex deposition process, a hybrid explicit-implicit FE methodology has been implemented using the commercial code ABAQUS 6.9. In a first stage, single particle impact at high velocity and peening is analyzed through an explicit FE formulation. The explicit FE analysis calculates the future state of a system based on its current state, providing comprehensive historical information of the stress and strain fields. This information is especially useful to model highly dynamic events subjected to considerably high strain rates and short periods of time, such as impacts, collisions or explosions (Systémes, 2009). In this case, the resulting peening stress caused by the impact is computed for different particle parameters (such as velocity, temperature, and morphology), as well as for substrate parameters (specifically, temperature). While an explicit formulation

is adequate for analyzing short periods of time, it is considerably costly in computational terms for longer time spans and repetitive impact (Systémes, 2009). Therefore, only a single impact is analyzed. Thus, in a second stage, the peening stresses profile computed initially are implemented in a thermomechanical layer deposition model based on an implicit FE formulation. Implicit FE analysis calculates the future state of a system solving an equation that includes both the current state and the future one, being more suitable for a wide range of problems over longer time spans. In this case, the layer deposition model by implicit FE computes the final residual stress condition due to peening, quenching, and thermal stresses after the addition of several layers. The methodology is summarized in Figure 1.

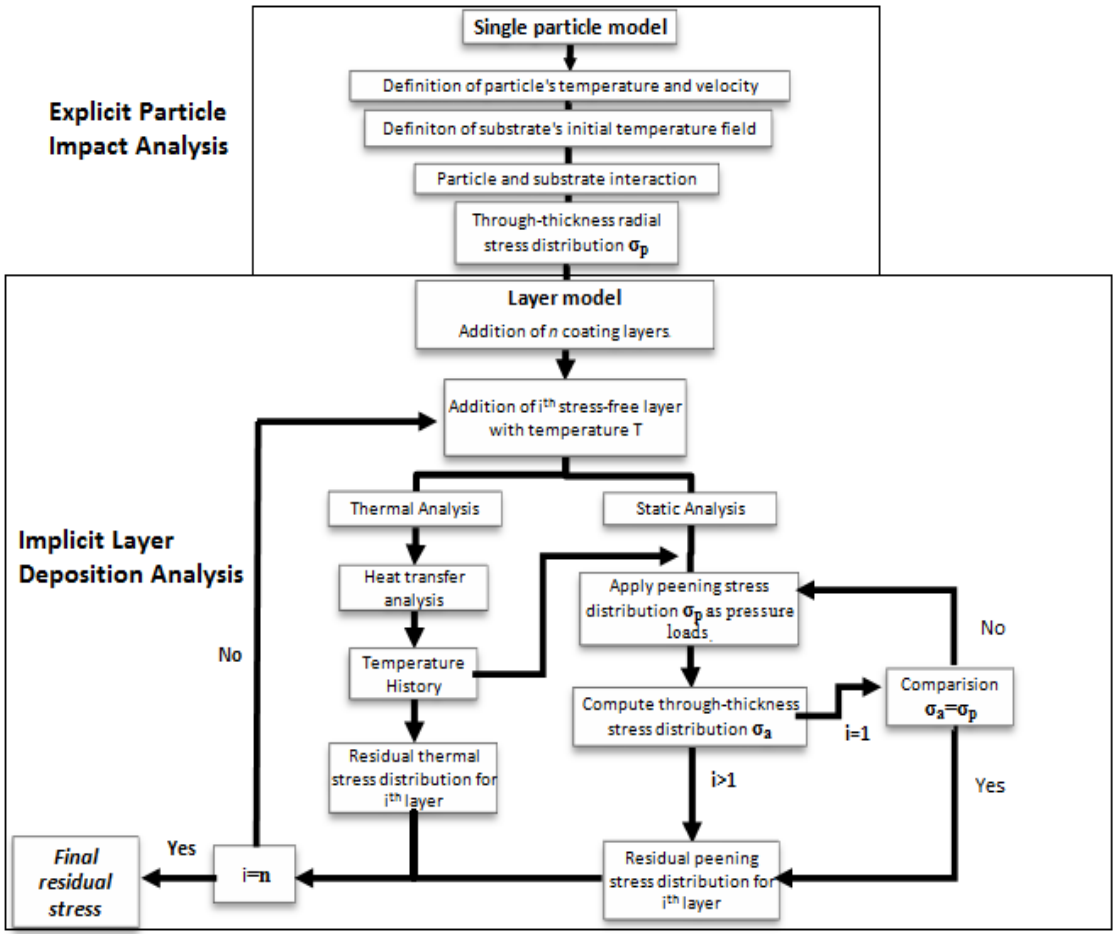

Figure 1: Flowchart of the hybrid explicit-implicit FE methodology of the model.

Explicit particle impact analysis.

A two-dimensional axisymmetric FE model of a stainless steel 316 (SS316) particle impacting on a cylindrical SS316 substrate was developed. The particle impact is analyzed as a dynamic coupled thermal-displacement phenomenon under high strain rates. It is assumed that particles do not interact between each other during the short time span of impact (e.g. there is no overlapping, or in-contact side-by-side impacts), and thus an independent single particle impact is a statistically representative event. The model considers initially the particle at a temperature significantly below the material's melting point. Thus, the particle impacts, deforms, and cools down all in solid state. With good approximation the

model considers 90% of the kinetic energy being transformed into heat (Hamid Assadi et al., 2003), with the rest of the energy being spent as 1) plastic deformation, 2) elastic wave energy, and 3) rebound kinetic energy (Bansal et al., 2007). Substrate dimensions are 1.5 mm radius and 1.5 mm thickness. The substrate dimensions, compared to particle's dimensions, are chosen to avoid edge effects. In addition, adequate symmetry boundary conditions are specified, and the nodes located at the bottom of the substrate are restrained. A prescribed temperature of 298 K is also defined at the bottom of the substrate, reflecting ambient temperature. The FE analysis assumes a no-separation criterion between the contacting nodes of the impinging particle and the substrate, therefore debonding or rebound is ruled out. This approach has been successful for modeling cold spray and other peening processes (Grujicic, Zhao, DeRosset, & Helfritch, 2004; Li et al., 2009). Particle and substrate are meshed employing quadrangular linear coupled temperature-displacement elements. The model is illustrated in Figure 2.

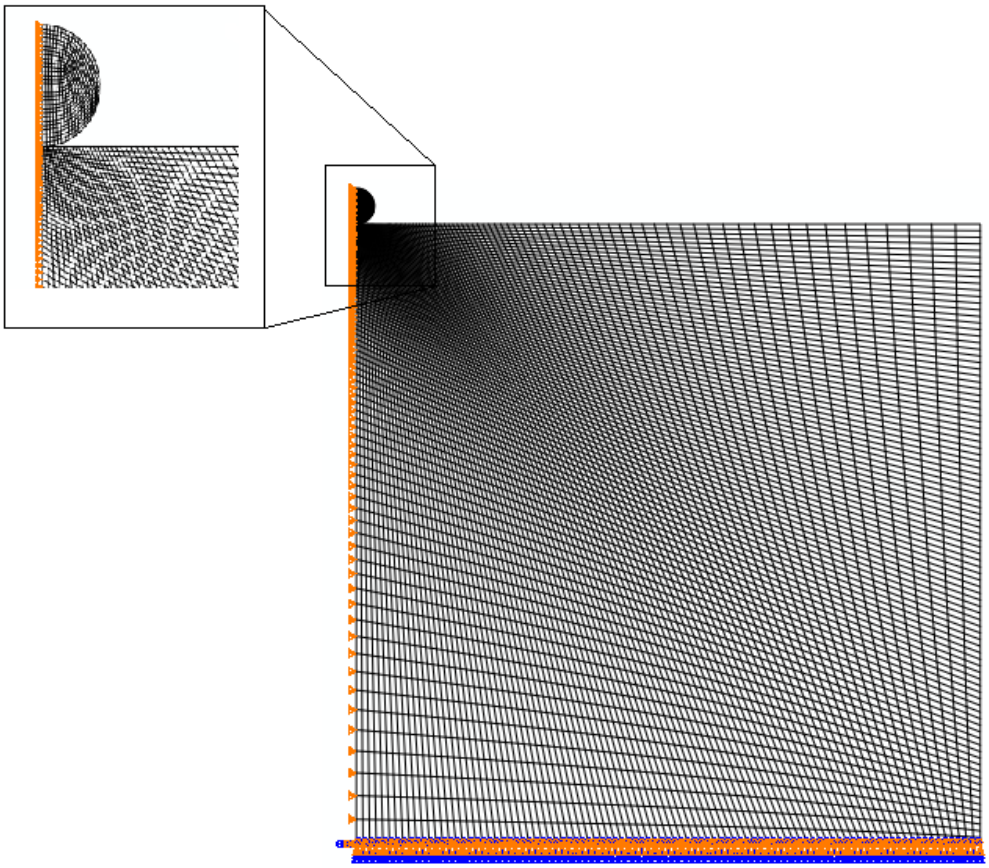

Figure 2: Axisymmetric single particle impact model

Impact is a non-linear phenomenon. Material properties for both particle and substrate have to account for temperature, strain and strain-rate dependence. For this case of solid impact, characterized by high temperature and high strain-rate, the appropriate constitutive equation is the Johnson-Cook (JC) model (Johnson & Cook, 1983). The stress σ in the plastic region is defined by the following equation:

$$\sigma = \left[A + B\left(\varepsilon_p\right)^n\right]\left[1 + Cln\left(\frac{\dot{\varepsilon_p}}{\dot{\varepsilon_{po}}}\right)\right]\left[1 - \left(\hat{T}\right)^m\right] \quad (1)$$

, where ε_p is the equivalent plastic strain, $\dot{\varepsilon_p}$ the equivalent plastic strain rate and $\dot{\varepsilon_{po}}$ the reference plastic strain rate measured at quasi-static conditions and at transition temperature T_o. A, B, C, m and n are material parameters. The parameter $\hat{T}$ corresponds to a non-dimensional temperature defined as:

$$\hat{T} = \begin{cases} 0, & T < T_o \\ \frac{T - T_o}{T_{melt} - T_o}, & T_{melt} \geq T \geq T_o \\ 1, & T > T_{melt} \end{cases} \quad (2)$$

, where T is the measured temperature and T_{melt} is the material's melt temperature.

JC properties for sprayed coating are not available in literature; in consequence, plastic properties for bulk SS316 are employed (Ghelichi, Bagherifard, Guagliano, & Verani, 2011; Marshall, 1984; Micunovic, Albertini, & Montagnani, 2003). It is assumed that impact properties do not differ considerably from those of the sprayed material (Totemeier, 2005). Additionally, SS316 bulk thermomechanical properties are used in those cases were appropriate data related to sprayed coating is not available. All relevant SS316 properties are summarized in Table 1. According to Equations 1 and 2, constitutive equations of SS316 JC model, the stress as a function of plastic strain under various strains rates and temperatures is shown in Figure 3.

Temperature Independent Properties	
Density (kg/m^3)	8031
Specific Heat ($J/kg \cdot K$)	457
Latent Heat of Fusion (J/kg)	3.30×10^5
Temperature Dependent Properties	
Temperature (K)	Elastic Modulus (GPa)
298	193
1500	100
1643	75
Temperature (K)	Thermal conductivity ($W/m^2 \cdot K$)
298	15
1500	30
1643	60
Temperature (K)	Thermal expansion coefficient ($1/K$)
298	1.60×10^{-5}
1500	1.85×10^{-5}
1643	3.00×10^{-5}

Table 1: Thermomechanical properties and JC model parameters for SS316.

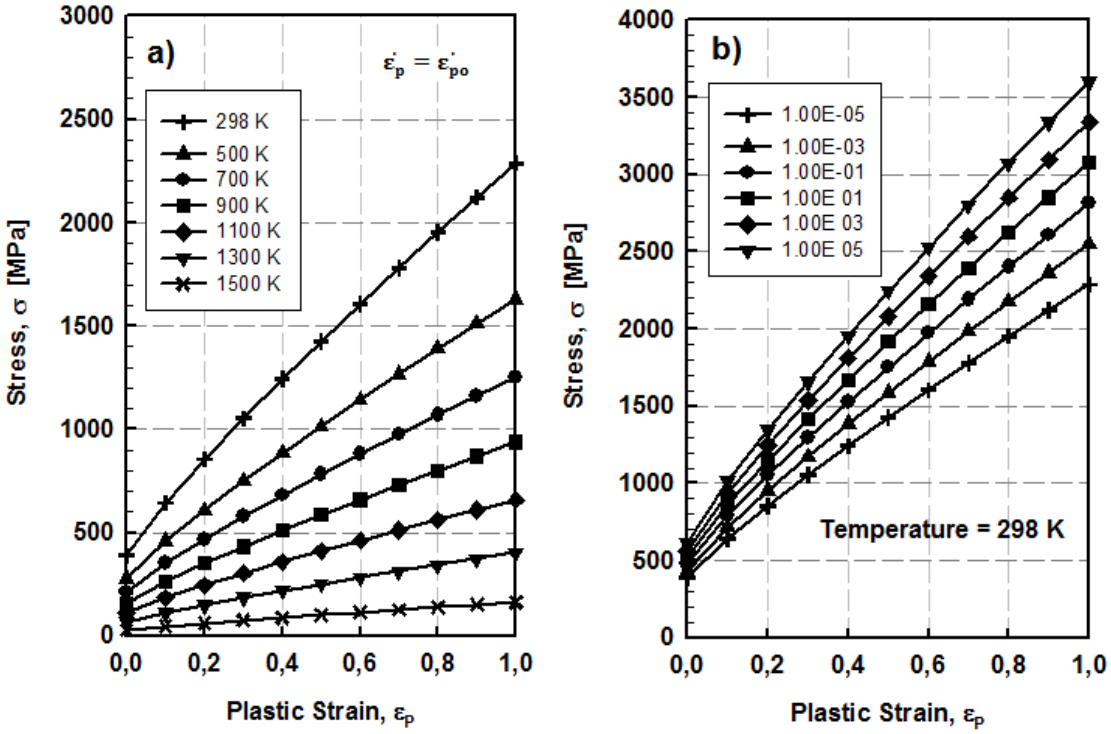

Figure 3: Stress as function of plastic strain for **a)** different temperatures and constant strain rate and **b)** different strain rates and constant temperature calculated through SS316 JC model.

As simulation output, the resulting radial residual stress $\sigma_r(z)$ distribution measured along the symmetry axis (the radial direction is defined as the in-plane direction) is computed after 400 ns of the onset of the impact. This time period is enough to allow for kinetic energy dissipation, particle spreading, substrate deformation and temperature stabilization.

Impact parametric analysis

The microstructure of thermal sprayed coatings is highly dependent on process parameters. The optimization of properties such as hardness, density, and elastic modulus is achieved by the appropriate combination of particle energy and deposition temperatures. The particle energy is defined by its kinetic energy and thermal energy. Therefore, it is appropriate to study the effect of particles at

different velocities, temperatures, sizes, and morphologies; over the residual stress profile. In this study, these parameters are tested individually within typical ranges.

The following physical parameters are varied for individual single impacts to observe the corresponding model response:

- **Particle velocity:** The particle velocity approaching perpendicular to the substrate surface at the impact time is varied between the values of 400 m/s, 500 m/s, 600 m/s, 700 m/s and 800 m/s.
- **Particle temperature:** The particle is assumed to have a homogeneous temperature distribution before impact. This temperature is varied with values of 800 K, 1000 K, 1200 K, 1400 K and 1600 K. However, it is noted that immediately after impact, the temperature is non-homogeneous in the particle due to heat generation and heat transfer to the substrate.
- **Particle mass:** The particle mass was varied by considering spherical particles of different diameters. Particles of 15 um, 30 um, 45 um, 60 um and 75 um in diameter are analyzed.
- **Particle morphology:** Fused-and-crushed powders usually include particles with sharp edges. To affect the particle morphology without changing considerably the impact dynamics and the particle kinetic energy, the particle mass is kept constant for different morphologies. In contrast to the previously adopted spherical shape, a rhomboidal particle is adopted to impact the substrate. To vary the particle morphology, the impact angle and mass are maintained constant

while the area moment of inertia with respect to the vertical axis is varied within values of 14.66 E03 μm^4, 16.59 E03 μm^4, 20.07 E03 μm^4, 23.89 E03 μm^4 and 28.04 E03 μm^4. The initial particle shapes and its corresponding area moment of inertia are shown in Figure 4. This approach makes possible to quantify the effect of mass distribution around the vertical axis without affecting other sensitive parameters.

- **Local deposition temperature**: Substrate temperature has been shown to significantly affect the cohesion strength between splats. Although this effect is not possible to be modeled since the cohesion between layers is assumed to be perfect, the effect over the residual stress buildup can be predicted. Substrate temperature has been found to be highly dependent on raster speed, part geometry, substrate cooling and especially on feed rate, as the latest can shorten the time between two overlying splats. Figure 5 shows the cooling curve of a single splat deposited on substrates of different overall temperature. The period of time after a second splat will find the previously deposited splat will depend on the feed rate. The higher the feed rate, the shorter the time and therefore, the higher the deposition temperature. Concurrently, as several layers of material are deposited and quenched on the substrate, the cooling process determines a temperature distribution in the specimen, and the highest temperature of this distribution corresponds to the region directly below the impact zone. This temperature is defined in this

work as the local deposition temperature and is varied within the values of 300 K, 600 K, 800 K and 1000 K. It is important to note that each temperature is linked to a specific temperature distribution that reduces linearly from the stated value at the substrate surface to the boundary condition of 298 K on the substrate bottom.

The reference condition at impact consists in a 30 um diameter spherical particle with impact velocity of 500 m/s. The particle temperature is 1600 K and the local deposition temperature is 300 K. To perform the parametric analysis, each physical quantity is varied independently while maintaining the rest of the reference parameters unaffected.

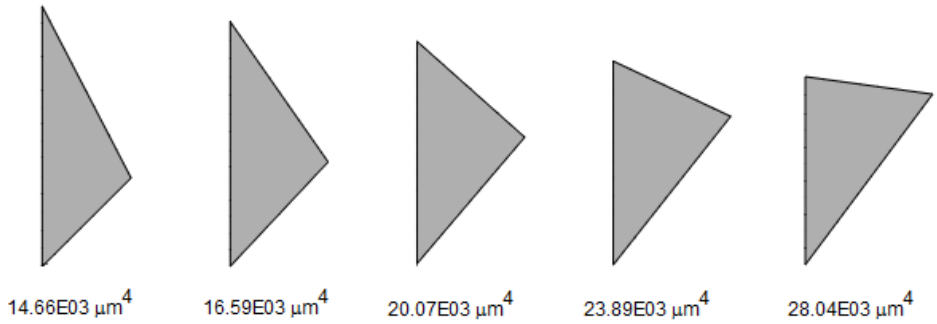

Figure 4: Axisymmetric particle shapes of equal mass and its calculated area moment of inertia with respect to the vertical axis.

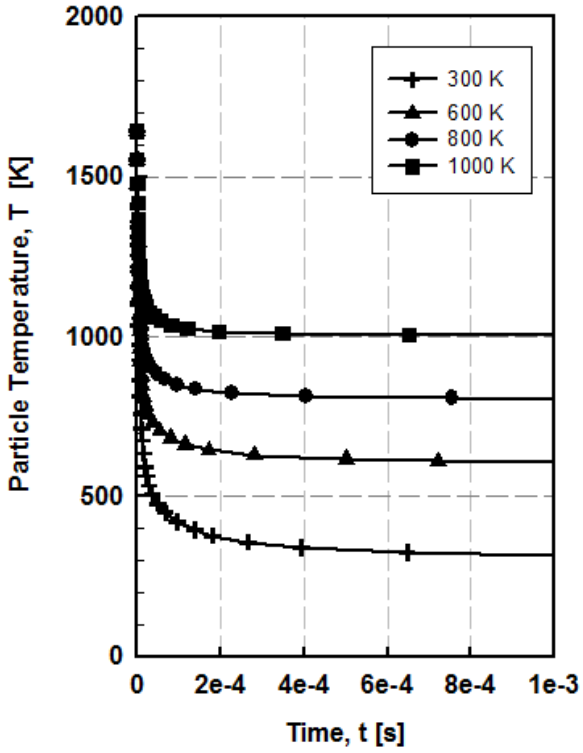

Figure 5: Cooling curves of a 10 um diameter splat for several overall substrate temperatures.

Implicit layer deposition analysis.

As stated previously, the rigorous explicit analysis is not adequate to model the coating process on a particle-by-particle impact basis. Further simplification based on an implicit methodology is required. In consequence, it is necessary to model the coating growth as a layer-by-layer deposition process of SS316. Here, a "layer" is defined as several splats of equal thickness aligned together along the substrate surface forming a complete slab of material. A two dimensional axisymmetric FE model is developed assuming that the residual stress profile under a single particle after the impact is repeatedly applied along the layer width. This model is shown in Figure 6. This imposition accounts for peening stresses during layer deposition. After this, an uncoupled thermal-mechanical analysis is

performed to calculate the thermal stress distribution developed due to quenching and post cooling, each time a whole layer of material cools down. A heat transfer simulation is initially performed to obtain the corresponding temperature history of the layer and substrate system, as illustrated in Figure 1. This temperature distribution is then used as an initial condition for a static analysis. The process is sequentially repeated for addition of each new layer.

Forty SS316 layers of 10 um thick each, corresponding to the observed final splat thickness after the explicit analysis, were deposited over a SS316 substrate cylinder of 2.0 mm. radius and 1.7 mm. thickness. A 100 ms delay is assumed between the arrival of each layer to account for gun displacement. To model heat transfer between the gas jet and the coating surface, a surface thermal load of 1 MW/m2 was applied during a time period of 39 ms, approximate transverse time span of the gun moving across the layer width. Convection cooling to ambient temperature is considered in all exposed surfaces of the specimen.

Temperature dependent thermomechanical properties, such as elastic modulus and thermal expansion coefficient, were taken from Table 1. The after deposition cooling process, depending of the specimen size, occurs in a long period of time compared to the actual deposition process. However, the quenching process is quite short. Thus, it is reasonable to consider the plastic response of the implicit model as strain-rate dependent and employ the previous JC model to characterize SS316 plastic properties. Finally, for heat transfer analysis, a mesh constituted of quadrangular linear heat transfer elements is employed; and for the stress analysis, a mesh constituted by quadrangular plane strain elements is employed.

To adequately implement peening stresses for the layer-by-layer model, it is necessary to repeatedly apply the explicit residual stress distribution along the layer width. To input the whole stress tensor iteratively is a tedious and time consuming process. A more efficient approach relies on applying just the in-plane stress component $\sigma_r(z)$ calculated during the explicit analysis as a pressure load $p(z)$ distribution that varies with depth z. The magnitude and direction of this $p(z)$ should induce in the implicit model a residual stress distribution $\sigma_{ri}(z)$ approximately equal to $\sigma_r(z)$. To achieve this similarity, a simple iterative process is used (Bansal et al., 2007). If $\sigma_{ri}(z)$ is the predicted residual stress when a radial $p_i(z)$ is applied during a hypothetical i_{th} iteration, an improved distribution is given by $p_{i+1}(z)$, calculated by the following equation:

$$p_{i+1}(z) = p_i(z) + \propto (\sigma_{ri}(z) - \sigma_r(z)) \quad (3)$$

, where α is weight coefficient considered, in this case, as 1. As illustrated in Figure 1, this iterative procedure is performed during the addition of the first layer of coating. After the similarity with respect to the explicit profile is achieved, the final pressure distribution $p_n(z)$ is subsequently applied for the addition of every layer. This procedure eventually calculates the final peening stress.

After the deposition simulation, the computed thermal stress distribution (quenching and post-cooling) is added to the peening stress distribution. Thus, a final residual stress distribution is obtained along the specimen depth. Through simple integration, it is possible to calculate the average stress in the coating zone. A parametric analysis is performed to study how these residual stress

distribution profiles and the average stress magnitudes vary with local deposition temperature and particle velocity (these two parameters are selected because they can be tailored during process control, and affect most significantly the stress profile, as it resulted from the single impact analysis). The methodical combination of these two parameters allows building a parameter map, and computing adequate results for each case. For the model purposes, the effect of particle velocity is accounted applying the appropriate stress distribution from the explicit analysis. Particle velocities of 400 m/s, 500 m/s, 600 m/s, 700 m/s and 800 m/s. The local deposition temperature is implemented by applying the appropriate temperature as an initial condition of the thermomechanical model. Local deposition temperatures of 300 K, 600 K, 800 K and 1000 K are considered.

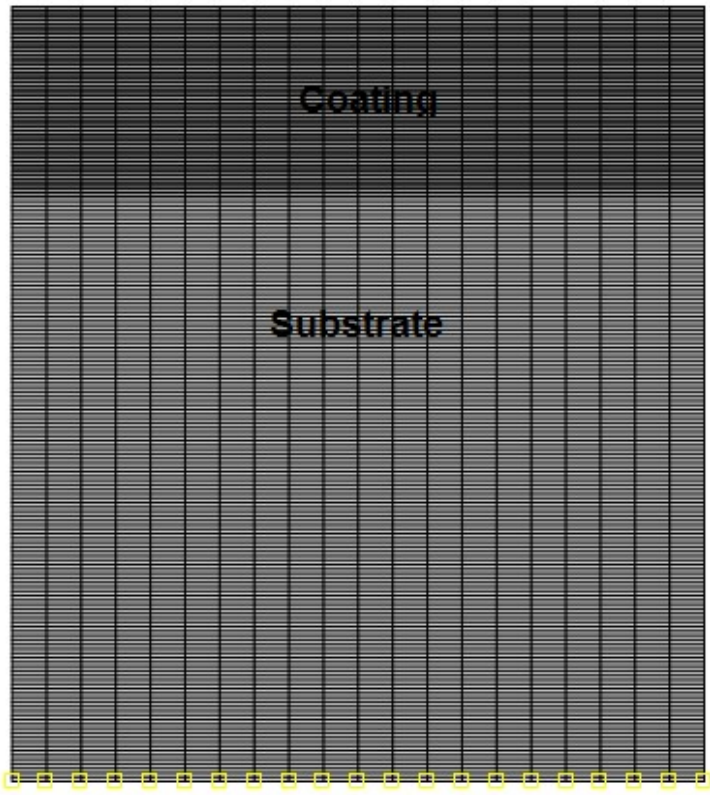

Figure 6: Axisymmetric implicit layer deposition model for SS316.

RESULTS

Individual particle effects on the stress profile

Figure 7 illustrates the deformed shape and the in-plane stress distribution of a single particle after impacting the substrate at different initial particle temperatures. After impact, the spherical particle turns into a splat of variable thickness and radius that spreads along the substrate according to its initial physical parameters. The overall shape and depth of the plastically deformed zone (or *impact crater*) in the substrate at a certain temperature defines the peening stress generated. In the following sections, the effect due to several parameters on in-plane peening stress during single particle impact is quantified.

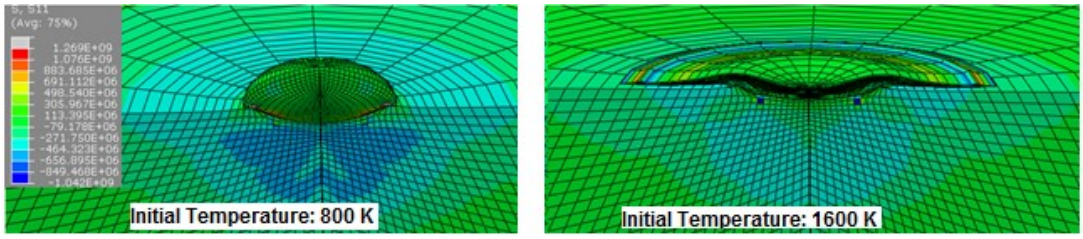

Figure 7: Splat shapes and residual in-plane stress field (in Pa) after impact for two particles whose initial temperatures are 800 [K] and 1600 [K].

A standard parameter is adopted for reference along the results section. This corresponds to an initial particle temperature 1600 [K], particle velocity 600 [m/s], local deposition temperature 298 [K], and particle size diameter of 30 [μm]. In Figure 7, the impact of two particles at different particle temperature is shown while maintaining the rest of the parameters the same as the standard condition.

Effects of particle state: velocity and temperature.

In this case, the kinetic and thermal energy of the particle is affected through variation of the physical parameters of particle velocity and temperature. Figure 8 shows the peening stress profile for impacts at several particle velocities. Higher particle velocity causes an increase in the maximum compressive stress. Also the substrate volume subjected to compressive stress tends to expand as the particle velocity increases. Both phenomena are directly related to higher penetration into the substrate.

Figure 9 shows the residual stress profile for several impacts of particles with initially different temperatures. The maximum compressive stress increases slightly for cooler particles. However, the stressed zone remains practically unchanged compared to cases where mass or velocity is varied (see Figure 8 and 10). During the impact process, it is observed that the final shape of the splat depends heavily on particle temperature. According to JC model, cooler particles suffer less plastic deformation than hotter particles, conserving a more spherical shape after impact.

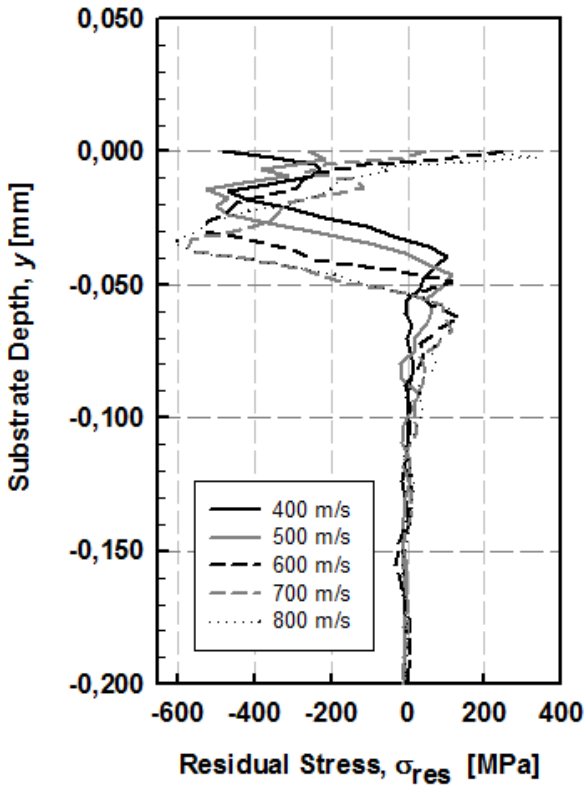

Figure 8: Residual in-plane stress as a function of substrate depth for different particle velocities[1].

[1] Other parameters are kept initially similar to the standard parameter.

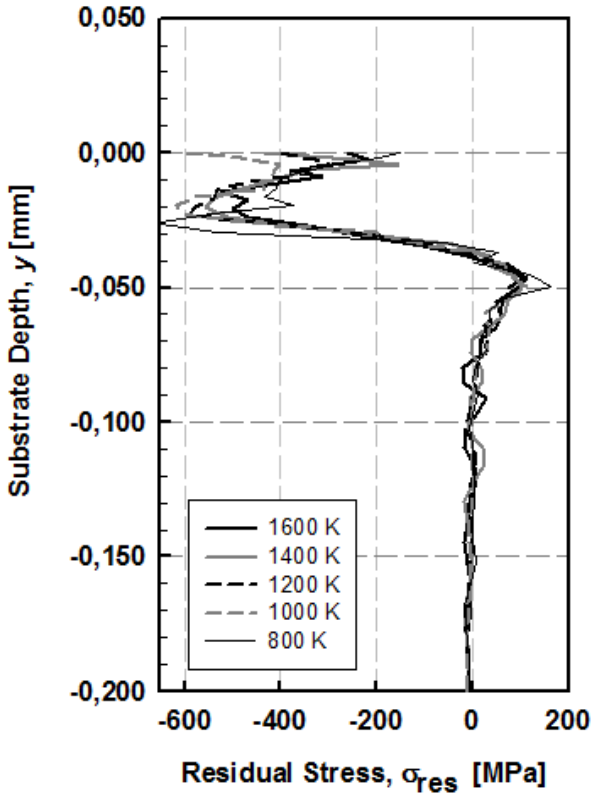

Figure 9: Residual in-plane stress as a function of substrate depth for different particle temperatures[2].

Effects of particle mass and morphology.

The variation of particle mass is studied by changing particle diameter. The particle is spherical in this case. It is noteworthy that a change in particle mass affects both kinetic and thermal energy. As seen in Figure 10, particles of higher mass increase the maximum compressive stress in the substrate significantly. The maximum value, around 550 MPa, seems to remain unchanged as the particle diameter surpasses 30 um. On the other hand, the substrate depth affected by compressive stress considerably increases with higher particle mass.

[2] Other parameters are kept initially similar to the standard parameter.

As stated before, the effect of particle morphology is analyzed considering the moment of inertia with respect to the vertical axis of a rhomboidal particle. Figure 11 shows the stress profile computed for particles of different moments of inertia. Kinetic and thermal energy is maintained constant in each case by employing particles of the same mass, velocity, and temperature. It is observed that particles with a lower area moment of inertia tend to penetrate deeper into the substrate and increase the maximum compressive stress right underneath the impact. This lower moment area of inertia is associated with sharp and collimated impacts. The plastic deformation zone after the impact of this type of particles was observed to be deep and shallow, explaining the observed shift in peak residual stress. In contrast, particles with higher area moments of inertia tend to have disperse and wider plastic deformation zones.

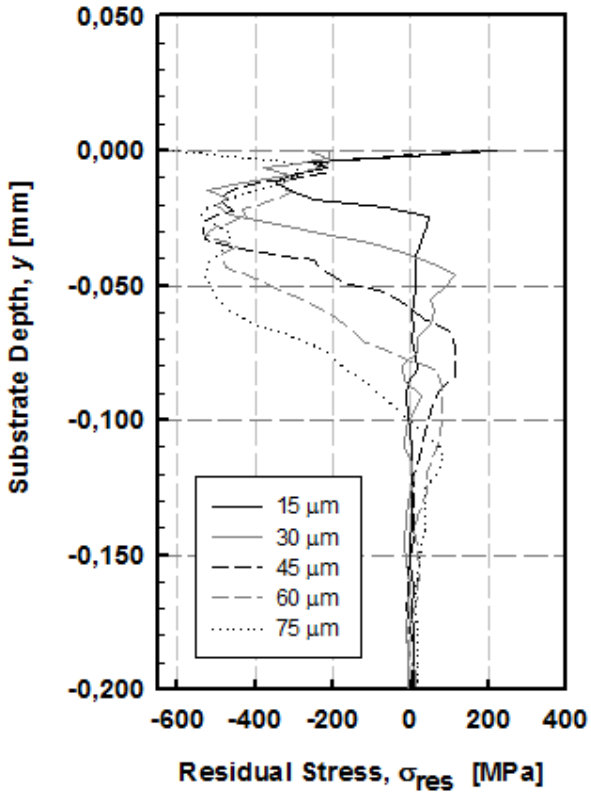

Figure 10: Residual in-plane stress as a function of substrate depth for different spherical particle diameters[3]

[3] Other parameters are kept initially similar to the standard parameter.

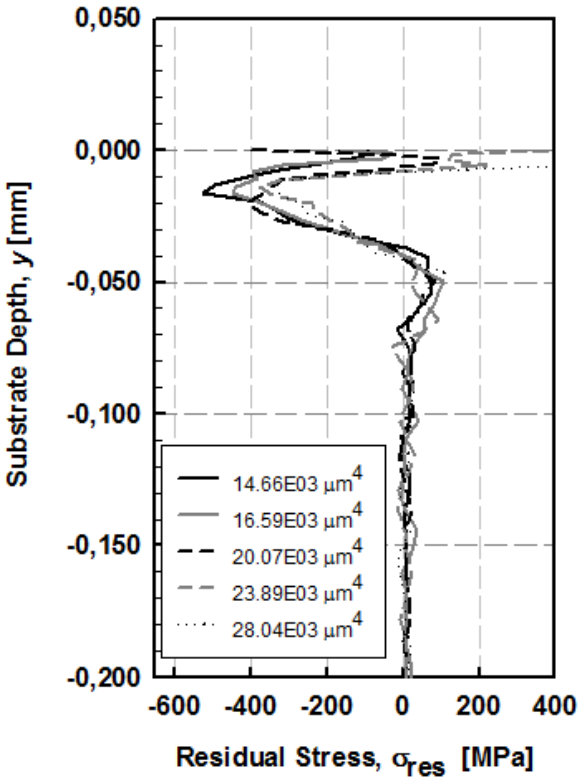

Figure 11: Residual in-plane stress as a function of substrate depth for different area moments of inertia with respect to vertical axis[4]

Effects of substrate condition: local deposition temperature.

The mechanical response of the substrate is analyzed considering several different local deposition temperatures. Figure 12 shows the stress profile for different local deposition temperatures. It is observed that the maximum compressive stress is achieved for lower substrate temperatures. This behavior is in agreement to the JC model, according to which plastic deformation at lower temperatures occurs at higher flow stress. The substrate volume affected by compressive stress spreads and increases slightly as the local deposition temperature increases.

[4] Other parameters are kept initially similar to the standard parameter.

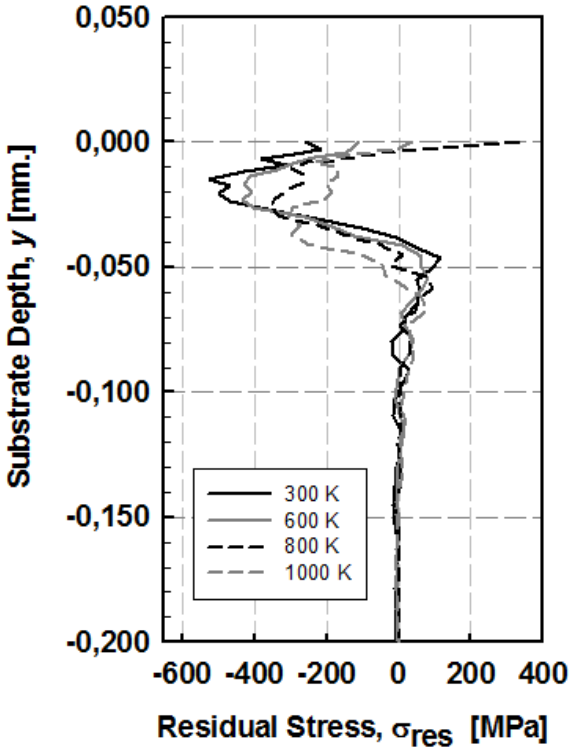

Figure 12: Residual in-plane stress as a function of substrate depth for different local deposition temperatures[5]

Through thickness residual stress profiles: response to local deposition temperature.

Two different profiles are computed via the layer-by-layer deposition model: quenching and thermal stress (

Figure 13a, which are actually both of thermal mismatch origin) and peening stress (

Figure 13b) for a particle at standard parameters (particle velocity of 500 m/s and temperature of 1600 K). Substrate deposition temperature (local deposition temperature) was the chosen parameter for analysis in this section

[5] Other parameters are kept initially similar to the standard parameter.

provided it showed and important effect over the impact and peening stress and it is known that it will also affect the quenching and thermal stresses.

Figure 13a shows that higher tensile stress in the coating zone is produced when local deposition temperature is high. This is explained by the higher thermal gradient through the thickness (hotter in the surface, cooler at the bottom) present as the specimen cools down to ambient temperature. It is also observed that the stress shift in the coating-substrate interface is more significant for higher local deposition temperatures. Compressive stress occurs all over the substrate in order to balance the tensile stress in the coating.

According to

Figure 13b, the compressive stress in the coating is higher for lower local deposition temperatures. This behavior agrees with the results observed for single particle impact as a function of local deposition temperature. The average value of stress along the coating is similar to the maximum compressive stress computed during single particle impact. In addition, it is observed that the peening stress does not have an important effect on the substrate stress profile (not after the first impact layers). This is explained by the short depth of the effect in single impacts inducing compressive stresses (around 0.05 mm.) compared to the substrate depth (1.7 mm.).

Figure 13c shows the superimposed total stress profile for several local deposition temperatures. Lower local deposition temperatures induce compressive stress in the coating, while higher temperatures induce tensile stress in the coating. As stated before, the effect is both explained by thermal and peening

stress evolution. The stress profile developed in the substrate is mainly an effect of the quenching phenomenon, and the sharp shift near the interface responds to both peening and quenching phenomena.

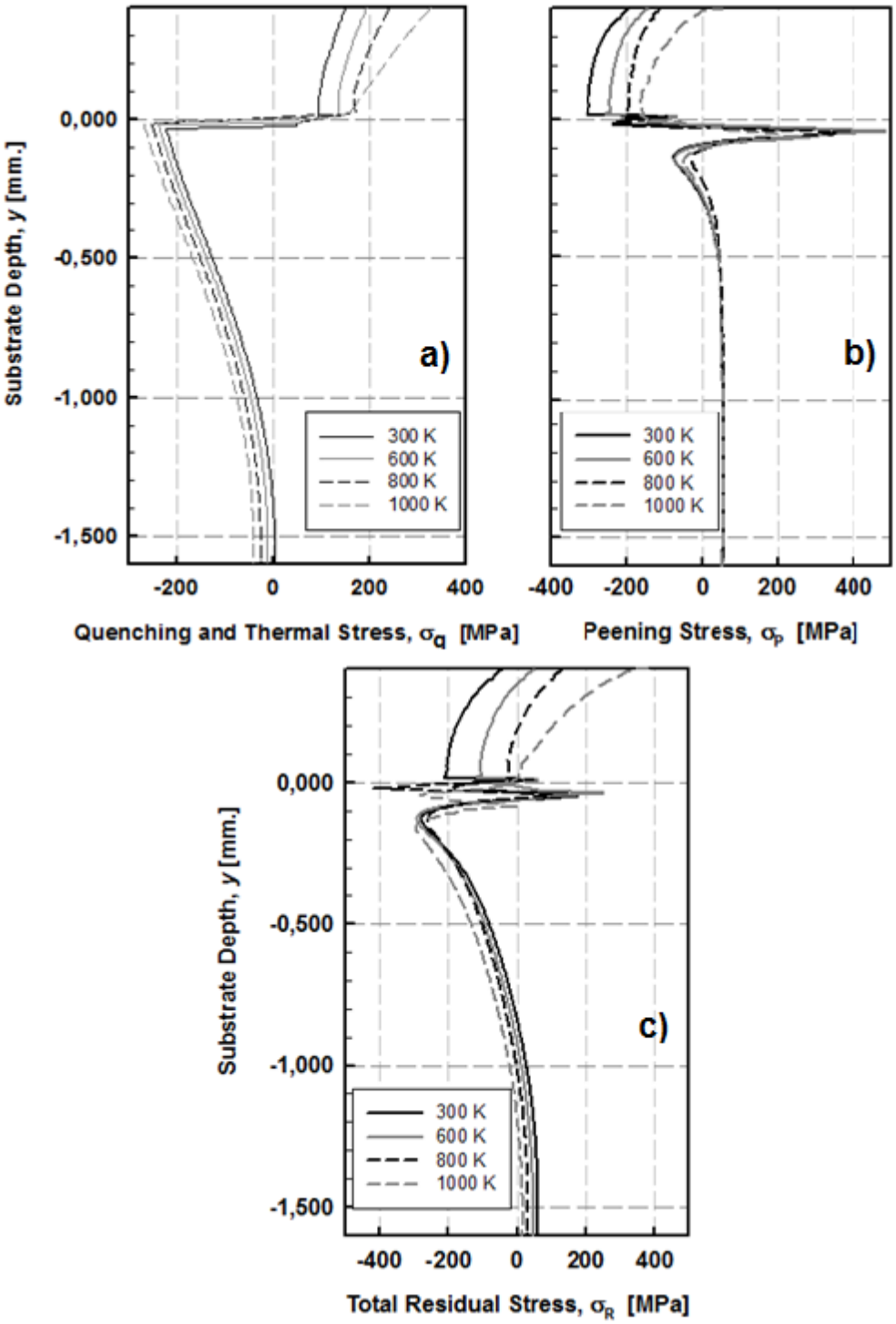

Figure 13: Quenching and thermal in-plane stress (a), peening in-plane stress (b) and total residual in-plane stress (c) as a function of substrate depth for different local deposition temperatures[6]

DISCUSSION

Single particle impact

The modeling results from individual impact conditions showed that the physical parameters that most affect the peening stress field in the in-plane direction are particle mass, local deposition temperature, and particle velocity. The effect of each of these parameters is summarized as follows:

a) Particle mass: larger particles induce larger maximum compressive stress. Also, the depth of stress field and the volume of the affected zone increases as the particle mass enhances.

b) Local deposition temperature: Higher local deposition temperature induces a lower maximum compressive residual stress after impact. In addition, the deepness of the stress affected zone increases for higher local deposition temperatures.

c) Particle velocity: the inherent increase in kinetic energy and strain rate associated with increments in particle velocity enhances the magnitude and depth of the maximum induced stress in the substrate. An increment in particle velocity, similarly way to the particle mass effect, increases the volume of the stress affected zone further into the substrate.

Theoretically, these behaviors are explained by the flow stress and its response to strain, strain rate and temperature according to the JC model. As

[6] Other parameters are kept initially equal to the standard parameter.

showed in Figure 3a, and Figure 3b respectively, the flow stress at a certain plastic strain increases with lower substrate temperatures and higher strain rates. On the other hand, kinetic energy increments, through mass or velocity increments, directly increase the strain rate during impact and enhance residual stress. Simulations based in flow stress models have shown similar results (Bansal et al., 2007; Yokoyama et al., 2006). In addition, both behaviors have been demonstrated experimentally for shot peening cases and are usually seen in a wide range of HV impact coating technologies (Kuroda et al., 2001; Lugscheider, Herbst, & Zhao, 1998; Pina, Dias, & Lebrun, 2003).

The other two physical parameters simulated, particle temperature and morphology, affect the residual stress field in a lower magnitude. In the case of particle temperature, the maximum stress showed just subtle differences for different impact conditions. These results might be related to explicit model limitations. As stated before, thermal stress is calculated through the implicit model. Since the explicit impact formulation only considers a small period of time (400 ns), heat transfer due to particle cooling is negligible during the explicit impact time span. Thus, an increase in particle thermal energy does not affect peening stress as much as a change in kinetic energy. However, if single particle quenching and cooling over a wider time span is considered, a notable difference in the final residual stress field might be expected. In the case of particle morphology, the differences in maximum stress values and in the shape of the plastically deformed zone are explained by the effect of mass distribution on impact dynamics. A sharper and collimated particle is observed to penetrate and deform deeply the substrate. Also, since the model outputs the residual stress field

along the particle central axis, those splats that have their mass closer to this axis (i.e. low area moment of inertia), will affect the peening stress in a more significant way compared to those with mass distributed further away from the center.

It seems that a change in kinetic energy or substrate conditions has more important effects on peening stress during single particle impact compared to changes in thermal energy or morphology. However, it must be considered that perfect adhesion between particle and substrate is an essential assumption of the model. Nevertheless, in real coating processes, some particles will bounce back and will not adhere to the substrate, leaving just a plastic deformed area after impact. This phenomenon occurs often when the impact physical parameters do not suffice a critical range, such as critical velocity or a minimal temperature (Kamnis, Gu, Lu, & Chen, 2009; Schmidt et al., 2006). Also, many factors are beyond the model's scope, such as: modeling the presence of oxide layers around the particle or substrate surface, the microstructural change during impact, non-homogenous substrate profiles, or multiphase materials, etc. In of all those cases, the effect of some physical parameters over single particle impact might differ from the ideal case.

Based on the results, it might be possible to generalize the effect of physical parameters of the process in order to tailor the peening stress distribution. For instance, in an attempt to produce coatings with favorable compressive stress for fatigue life increase, it is observed that the most influential factor could be to increase particle size (e.g. by altering the feedstock or powder preparation process), reduce local deposition temperature (e.g. by decreasing feed rate or adding external cooling), or increasing particle velocity (e.g. by increasing torch

gas flows). There exists, on the other hand, hardware considerations that may limit the modification of these variables, for instance increasing particle size may produce incomplete melting in large particles (Stoltenhoff, Kreye, & Richter, 2002); at low feed rates, low deposition efficiency may be attained (Gilmore, Dykhuizen, Neiser, Smith, & Roemer, 1999); and powder optimization can be complex (Fauchais, Montavon, & Bertrand, 2010), etc. Also, the coating and substrate materials could impose certain limitations over coating quality and microstructure, reducing the range in which some processing parameters might be varied. In consequence, the results produced in this section suggest pathways or frameworks for HV impact coating design rather than specific hardware optimization measures. Appropriate scientific methodologies such as process maps (Sampath et al., 2003) or design-of-experiments (Pierlot, Pawlowski, Bigan, & Chagnon, 2008), based on appropriate experimental data, should be applied to optimize process parameters for specific coating technologies and sprayed materials.

Through thickness residual stress profiles

As stated previously, the implemented layer-by-layer model allows analyzing separately the quenching and thermal stress, and the peening stress profiles. Calculated quenching and thermal stress profiles show the effect of several local deposition temperatures (

Figure 13a). Higher local deposition temperatures are translated into higher overall thermal mismatch after the cooling process, thus higher tensile stress is

developed in the coating while higher compressive stress is developed in the substrate. It should be noted that some assumptions in the model may produce a different response than in the actual coating deposition. Assumptions such as: ideal thermal conductance between each layer, perfect bonding between splats and the effect of JC model properties must be considered. In a real HV impact processes, the complex microstructure, porosity and non-ideal physical interfaces between each successive coated layer could act as thermal barriers for heat dissipation, sliding interfaces that relief stress, etc (Ravichandran, An, Dutton, & Semiatin, 1999). Thus, the temperature after coating deposition of the specimen and its inherent thermal mismatch could be higher than the ideal case. In consequence, in certain cases where non-ideally thermal interfaces have a considerable effect, the current model might underestimate the thermal stress after cooling. Besides this fact, as stated by the JC model (Figure 3a), the flow stress at a certain plastic strain reduces significantly with temperature. The stress associated with a certain temperature gradient during quenching is diminished as the area directly under the layer gets hotter. This behavior might be expected for metals defined by JC constitutive equation. In the opposite case, if the JC model parameters state that the stress does not change significantly with temperature (e.g. cermets and ceramics: WC-Co, CrC-NiCr, Al_2O_3), the expected quenching effect should be high. Many times the high residual stress produces cracking of the coating *in situ* during deposition. Accordingly, the difference of thermal stress profiles observed when comparing quenching and cooling at different temperature gradients is material specific.

Through thickness peening stress profiles shown in

Figure 13b are consistent with the results from single particle impact (Figure 12). Differences between both cases are explained by the stress balance throughout the substrate during the implicit simulation. The effect of local deposition temperature on compressive stress is clear. Nevertheless, the effect of non-ideal deposition efficiency and other complex impact conditions must be taken into account. The layer-by-layer model assumes that the particle impact that considers perpendicular trajectory, non interaction, and perfect adhesion conditions is statistically significant; thus, it is possible to extrapolate single particle impact results along the whole layer width. However, in the real coating process, this might not be the case. Even in controlled conditions, the effect of low deposition efficiencies, and other impact conditions (splashing, particle oxidation, surface oxidation, etc.) will have an effect over the peening stress profile. Further developments of the current model should include the influence of these non-ideal conditions in combination with an adequate statistical framework (Hong, Ooi, & Shaw, 2008). Moreover, the model does not account for stress relaxation mechanisms such as material damage, creep or cracking after the particle impact takes place (Dalmas et al., 2003). Neither the known tendency to improve inter-splat bonding between splats at high substrate temperature is possible to be modeled, as the study assumes perfect bonding. Considering these limitations of the model, peening stress was systematically estimated theoretically in this study.

Final through thickness residual stress profiles shown in

Figure 13c and the associated effect of several local deposition temperatures are presented. Both “peening” and “quenching and thermal” stress profiles are shown to affect the final residual stress distribution. This influence is

consistent with most of HV impact processes when considering the magnitude of the stresses, range of velocities and local deposition temperatures. It is shown that it is possible to tailor the final residual stress distribution and increase the coating quality by several approaches. First, the residual stress profiles show a shift of stress in the coating/substrate interface. In the works of (Clyne & Gill, 1996; Godoy et al., 2002; Howard et al., 1994), this misfit has been related to coating debonding probability by the fundamental parameter known as *strain energy release rate*. In the case of a thin coating or deposit subjected to a residual stress distribution, the strain energy release rate G consists in the stored elastic strain energy per unit of interfacial area, defined by the following equation:

$$G = \frac{{\sigma_c}^2 h}{2E_c} + \frac{{\sigma_s}^2 H}{2E_s} \quad (4)$$

, where σ_c and σ_s are the stress on coating and on substrate at the interface respectively, E_c and E_s are the Young moduli of coating and substrate respectively, and h and H correspond to coating and substrate thickness respectively. Theoretically, spontaneous debonding occurs when the strain energy release rate G reaches a critical value G_{ic}, which is closely related to fracture toughness K_{ic}. Process design to avoid spontaneous debonding should reduce the misfit in the coating/substrate interface. As shown by

Figure 13c, an adequate selection of lower local deposition temperature (or higher particle velocities), achieved by varying either feed rate or gas flow, will

affect σ_c and σ_f, decreasing the stress misfit and the inherent debonding probability.

Second, it is possible to positively affect fatigue life and other mechanical properties through suitable parameter configurations. A highly compressive stress in coating could increase fatigue life dramatically. In experiments conducted by (McGrann et al., 1998), it has been showed that residual stress in steel and aluminum coatings affects fatigue life by a factor of ten. It is proposed that the superimposed residual stress in the coating and in the top layers of the substrate help delay crack initiation. In addition, vertical crack propagation at initial state is significantly constrained by compression in crack surroundings. Accordingly, selection of hardware parameters should favor a compressive residual stress distribution in coating for this purpose.

Correlation between parameters

It is often observed that manipulation of process parameters determine effects over particle state and local deposition temperature simultaneously, for instance changing oxygen flow or fuel flow in HVOF, influences the length of the flame torch and therefore, the heat input into the substrate. In consideration of this, it is discussed in the following section the parametric combination of two of the most influencing factors: particle velocity and substrate temperature in the range of HV impact coatings. The rest of parameters (particle mass, morphology and temperature) are maintained in its corresponding reference values. From the point of view of hardware control, it is regularly observed that manipulation of particle

velocity determines a change in local deposition temperature in the substrate. For this reason, the effects of both parameters occurring simultaneously are studied in more detail.

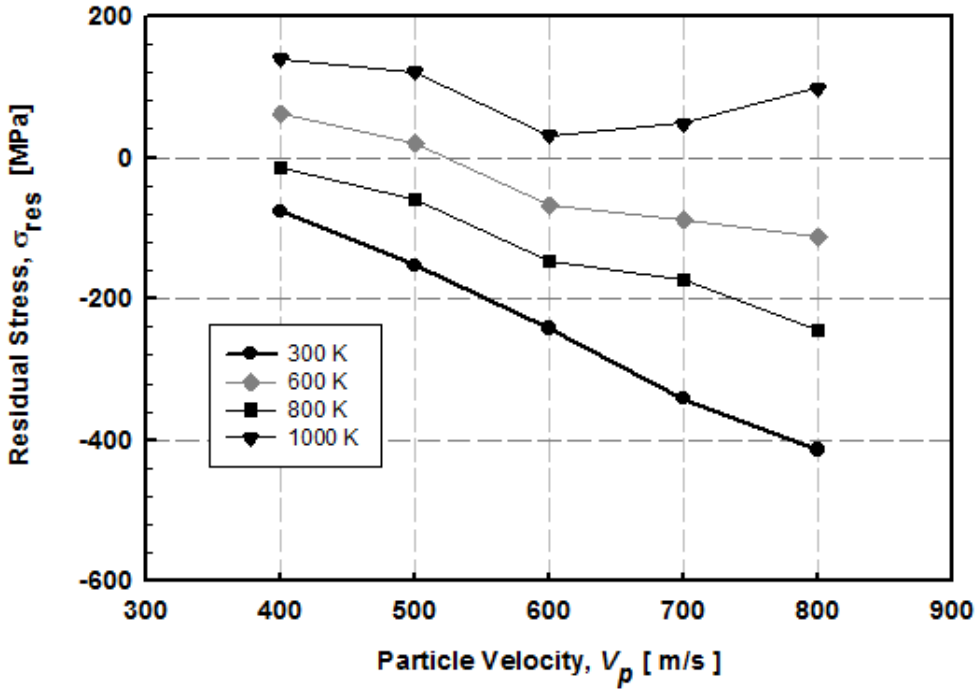

Figure 14: Average in-plane residual stress in coating as a function of particle velocity for different local deposition temperatures.

Figure 14 illustrates the effect of particle velocity over total average residual stress in coating for different deposition temperatures. A linear and monotonically decreasing tendency is observed. This trend is confirmed by experimental data for various coating process. As stated by the JC model in Figure 3a, the stress corresponding to a certain temperature shows a clear decreasing trend in constant intervals in the range of 300 K to 1000 K. In general, this behavior is observed as well for average residual stress. Coating deposition at the highest local deposition temperature (1000 K) shows a deviation from the expected tendency at the

highest particle velocity. This deviation might be associated to convergence problems as the model considers more extreme temperature magnitudes, becoming more sensitive to strain rate effects.

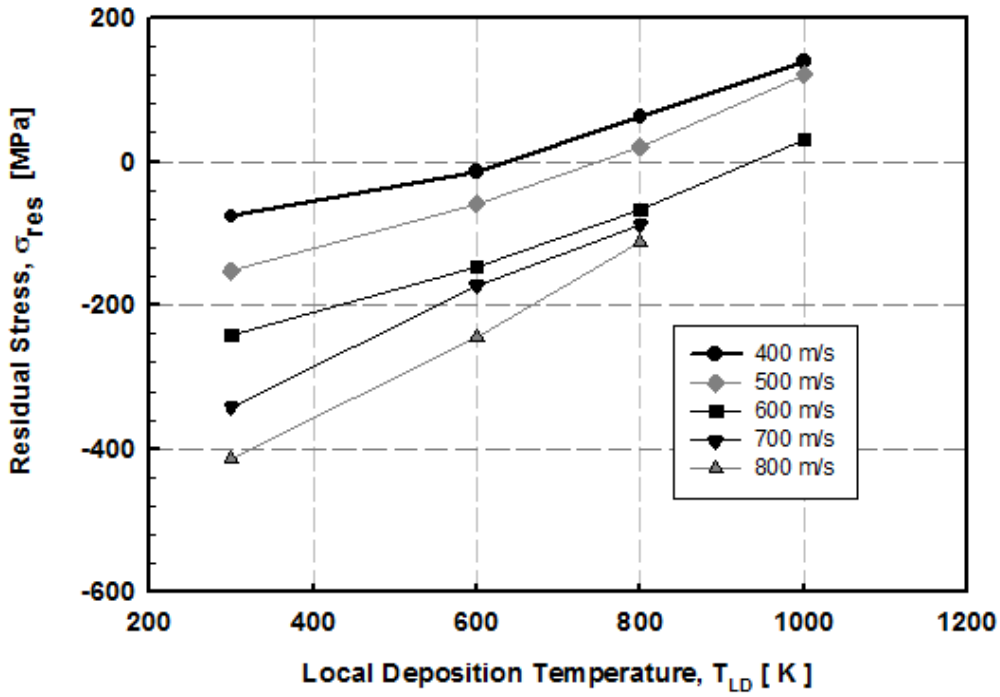

Figure 15: Average in-plane residual stress in coating as a function of local deposition temperatures for different particle velocities.

Similarly, Figure 15 illustrates the effect of local deposition temperature over total average residual stress in coating for different particle velocities. A linear, monotonically increasing tendency is observed in this case. This trend is also confirmed by experimental data for various coating processes. As stated by the JC model in Figure 3b, the stress associated to a certain strain rate shows a clear decreasing trend in constant intervals, but this change is low compared to the previously analyzed temperature effects. Compared to Figure 14, average residual stress calculated by the layer-by-layer model is thus consistent with the

observed JC trend. Nevertheless, coating deposition at the highest particle velocities and local deposition temperatures (>700 m/s, >800 K) shows a deviation from the expected tendency. Again, this deviation might be associated with convergence issues and JC model limitations as the strain rate and temperature approaches extreme values.

Figure 14 and Figure 15 show tendencies individually for the studied parameters. In an attempt to observe together the effects of both particle state and deposition temperature, the average residual stress in coating is mapped for both paramets in Figure 16. In general, the mapping methodology here allows process designers to select regions of desired residual stresses on the map, to choose hardware parameters and reproduce particle state and deposition temperature.

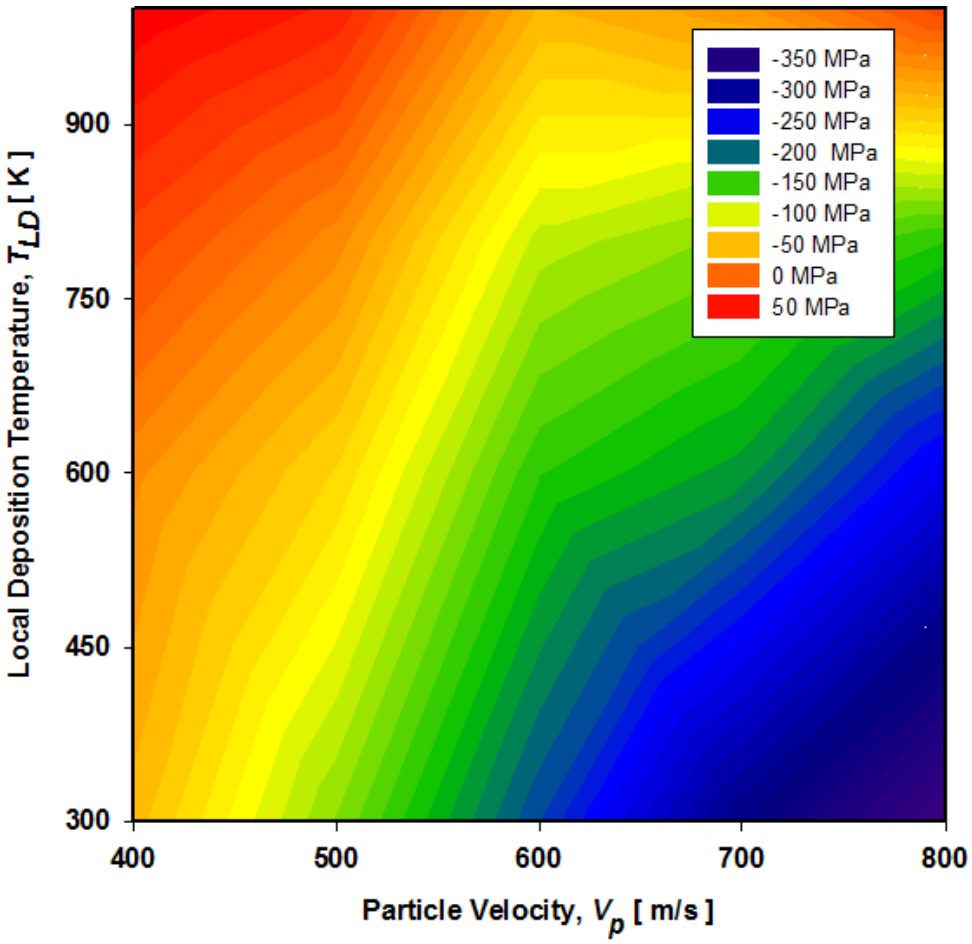

Figure 16: Contour map of average residual stress in coating as a function of local deposition temperature and particle velocity.

A clear tendency exists for both independent variables. Fast speed of particles at lower deposition temperature define high compressive stress, whereas low speed and higher lower deposition temperature reduce the stress towards tensile. Accordingly, there coud be a chance to spray layers of optimum neutral residual stress, employing mean local deposition temperatures (around 650 K to 700 K) and low particle velocities (around 400 m/s to 500 m/s). Adequate proccess design could tailor the average residual stress around these values, but it must be

considered that mainting hardware parameters consistently in this small range during deposition might be challenging in some technologies.

Moreover, the results of this section are consistent with behavior stated with JC model. This consistency might allow generalizing the observed tendency for other materials with similar JC model parameters and expanding the model beyond SS316 simulation. For instance, a wide spectrum of ductile metals could be considered without major complication and a similarity in trends could be expected. Nevertheless, for more complex microstructures or extremely different JC model definitions, it might not be possible to perform this generalization.

CONCLUSIONS

In order to predict and favor certain tendencies in residual stress distributions in HV impact coatings, a hybrid explicit-implicit FE methodology has been implemented. A parametric study has been performed in order to estimate the effect of physical parameters over peening stress, quenching and thermal stress and final residual stress. The effects of particle velocity, mass, temperature,

morphology and substrate temperature over peening profiles were investigated for single particle impact; while, for coating growth and deposition, the effect of particle velocity and local deposition temperature over total residual stress is emphasized. In both cases, the stress results magnitudes and trends are consistent with experimental data from literature. The effect of both “peening” and “quenching and thermal” residual stress distribution to tailor final stress is highlighted. These results provide a framework to relate physical variables with hardware parameters in order to attain desired residual stress conditions in the coating and furthermore a desired stress profile. Correct manipulation of residual stress allows for improvements in adhesion, fatigue life and crack propagation.

REFERENCES

Assadi, H., Gärtner, F., Stoltenhoff, T., & Kreye, H. (2003). Bonding mechanism in cold gas spraying. *Acta Materialia, 51*(15), 4379-4394. doi: http://dx.doi.org/10.1016/S1359-6454(03)00274-X

Assadi, H., Schmidt, T., Richter, H., Kliemann, J.-O., Binder, K., Gärtner, F., . . . Kreye, H. (2011). On parameter selection in cold spraying. *Journal of thermal spray technology, 20*(6), 1161-1176.

Bansal, P., Shipway, P. H., & Leen, S. B. (2007). Residual stresses in high-velocity oxy-fuel thermally sprayed coatings – Modelling the effect of particle velocity and temperature during the spraying process. *Acta Materialia, 55*(15), 5089-5101. doi: http://dx.doi.org/10.1016/j.actamat.2007.05.031

Bemporad, E., Sebastiani, M., Casadei, F., & Carassiti, F. (2007). Modelling, production and characterisation of duplex coatings (HVOF and PVD) on Ti–6Al–4V substrate for specific mechanical applications. *Surface and Coatings Technology, 201*(18), 7652-7662. doi: http://dx.doi.org/10.1016/j.surfcoat.2007.02.041

Buchmann, M., Gadow, R., & Tabellion, J. (2000). Experimental and numerical residual stress analysis of layer coated composites. *Materials Science and Engineering: A, 288*(2), 154-159.

Clyne, T., & Gill, S. (1996). Residual stresses in thermal spray coatings and their effect on interfacial adhesion: a review of recent work. *Journal of thermal spray technology, 5*(4), 401-418.

Dalmas, D., Benmedhakene, S., Kebir, H., Richard, C., Laksimi, A., & Roleandt, J. (2003). Investigation of failure mechanisms in WC–Co coated materials. *Surface and Coatings Technology, 173*(2), 130-143.

Fauchais, P., Montavon, G., & Bertrand, G. (2010). From powders to thermally sprayed coatings. *Journal of thermal spray technology, 19*(1-2), 56-80.

Frija, M., Hassine, T., Fathallah, R., Bouraoui, C., & Dogui, A. (2006). Finite element modelling of shot peening process: Prediction of the compressive residual stresses, the plastic deformations and the surface integrity. *Materials Science and Engineering: A, 426*(1–2), 173-180. doi: http://dx.doi.org/10.1016/j.msea.2006.03.097

Ghafouri-Azar, R., Mostaghimi, J., & Chandra, S. (2006). Modeling development of residual stresses in thermal spray coatings. *Computational Materials Science, 35*(1), 13-26. doi: http://dx.doi.org/10.1016/j.commatsci.2005.02.007

Ghelichi, R., Bagherifard, S., Guagliano, M., & Verani, M. (2011). Numerical simulation of cold spray coating. *Surface and Coatings Technology, 205*(23), 5294-5301.

Gilmore, D., Dykhuizen, R., Neiser, R., Smith, M., & Roemer, T. (1999). Particle velocity and deposition efficiency in the cold spray process. *Journal of thermal spray technology, 8*(4), 576-582.

Godoy, C., Souza, E. A., Lima, M. M., & Batista, J. C. A. (2002). Correlation between residual stresses and adhesion of plasma sprayed coatings: effects of a post-annealing treatment. *Thin Solid Films, 420–421*(0), 438-445. doi: http://dx.doi.org/10.1016/S0040-6090(02)00805-2

Grujicic, M., Zhao, C. L., DeRosset, W. S., & Helfritch, D. (2004). Adiabatic shear instability based mechanism for particles/substrate bonding in the cold-gas dynamic-spray process. *Materials & Design, 25*(8), 681-688. doi: http://dx.doi.org/10.1016/j.matdes.2004.03.008

Hong, T., Ooi, J. Y., & Shaw, B. (2008). A numerical simulation to relate the shot peening parameters to the induced residual stresses. *Engineering Failure Analysis, 15*(8), 1097-1110. doi: http://dx.doi.org/10.1016/j.engfailanal.2007.11.017

Howard, S. J., Tsui, Y. C., & Clyne, T. W. (1994). The effect of residual stresses on the debonding of coatings—I. A model for delamination at a bimaterial interface. *Acta Metallurgica et Materialia, 42*(8), 2823-2836. doi: http://dx.doi.org/10.1016/0956-7151(94)90223-2

Johnson, G. R., & Cook, W. H. (1983). *A constitutive model and data for metals subjected to large strains, high strain rates and high temperatures.* Paper presented at the Proceedings of the 7th International Symposium on Ballistics.

Kamnis, S., Gu, S., Lu, T. J., & Chen, C. (2009). Numerical modeling the bonding mechanism of HVOF sprayed particles. *Computational Materials Science, 46*(4), 1038-1043. doi: http://dx.doi.org/10.1016/j.commatsci.2009.05.009

Kuroda, S., Tashiro, Y., Yumoto, H., Taira, S., Fukanuma, H., & Tobe, S. (2001). Peening action and residual stresses in high-velocity oxygen fuel thermal spraying of 316L stainless steel. *Journal of thermal spray technology, 10*(2), 367-374.

Li, W.-Y., Zhang, C., Li, C.-J., & Liao, H. (2009). Modeling Aspects of High Velocity Impact of Particles in Cold Spraying by Explicit Finite Element Analysis. *Journal of thermal spray technology, 18*(5-6), 921-933.

Lugscheider, E., Herbst, C., & Zhao, L. (1998). Parameter studies on high-velocity oxy-fuel spraying of MCrAlY coatings. *Surface and Coatings Technology, 108*, 16-23.

Marshall, P. (1984). Austenitic stainless steels: microstructure and mechanical properties: Springer.

McGrann, R. T. R., Greving, D. J., Shadley, J. R., Rybicki, E. F., Kruecke, T. L., & Bodger, B. E. (1998). The effect of coating residual stress on the fatigue life of thermal spray-coated steel and aluminum. *Surface and Coatings*

Technology, 108–109(0), 59-64. doi: http://dx.doi.org/10.1016/S0257-8972(98)00665-3

Meguid, S. A., Shagal, G., & Stranart, J. C. (1999). Finite element modelling of shot-peening residual stresses. *Journal of Materials Processing Technology, 92–93*(0), 401-404. doi: http://dx.doi.org/10.1016/S0924-0136(99)00153-3

Meguid, S. A., Shagal, G., & Stranart, J. C. (2002). 3D FE analysis of peening of strain-rate sensitive materials using multiple impingement model. *International Journal of Impact Engineering, 27*(2), 119-134. doi: http://dx.doi.org/10.1016/S0734-743X(01)00043-4

Micunovic, M., Albertini, C., & Montagnani, M. (2003). High strain rate thermo-inelasticity of damaged AISI 316H. *International Journal of Damage Mechanics, 12*(4), 267-303.

Ng, H. W., & Gan, Z. (2005). A finite element analysis technique for predicting as-sprayed residual stresses generated by the plasma spray coating process. *Finite Elements in Analysis and Design, 41*(13), 1235-1254. doi: http://dx.doi.org/10.1016/j.finel.2005.02.002

Phan, T. D., Masood, S. H., Jahedi, M. Z., & Zahiri, S. (2010). *Residual stresses in cold spray process using finite element analysis.* Paper presented at the Materials Science Forum.

Pierlot, C., Pawlowski, L., Bigan, M., & Chagnon, P. (2008). Design of experiments in thermal spraying: A review. *Surface and Coatings Technology, 202*(18), 4483-4490.

Pina, J., Dias, A., & Lebrun, J. (2003). Study by X-ray diffraction and mechanical analysis of the residual stress generation during thermal spraying. *Materials Science and Engineering: A, 347*(1), 21-31.

Ravichandran, K. S., An, K., Dutton, R. E., & Semiatin, S. (1999). Thermal Conductivity of Plasma-Sprayed Monolithic and Multilayer Coatings of Alumina and Yttria-Stabilized Zirconia. *Journal of the American Ceramic Society, 82*(3), 673-682.

Sampath, S., Jiang, X., Kulkarni, A., Matejicek, J., Gilmore, D., & Neiser, R. (2003). Development of process maps for plasma spray: case study for molybdenum. *Materials Science and Engineering: A, 348*(1), 54-66.

Schmidt, T., Gärtner, F., Assadi, H., & Kreye, H. (2006). Development of a generalized parameter window for cold spray deposition. *Acta Materialia, 54*(3), 729-742. doi: http://dx.doi.org/10.1016/j.actamat.2005.10.005

Stoltenhoff, T., Kreye, H., & Richter, H. (2002). An analysis of the cold spray process and its coatings. *Journal of thermal spray technology, 11*(4), 542-550.

Systémes, D. (2009). Abaqus 6.9 Theory Manual. *Dassault Systémes Simulia Corp., RI, USA*.

Thornton, C., & Yin, K. K. (1991). Impact of elastic spheres with and without adhesion. *Powder Technology, 65*(1–3), 153-166. doi: http://dx.doi.org/10.1016/0032-5910(91)80178-L

Toparli, M., Sen, F., Culha, O., & Celik, E. (2007). Thermal stress analysis of HVOF sprayed WC–Co/NiAl multilayer coatings on stainless steel substrate using finite element methods. *Journal of Materials Processing Technology, 190*(1–3), 26-32. doi: http://dx.doi.org/10.1016/j.jmatprotec.2007.03.115

Totemeier, T. C. (2005). Effect of high-velocity oxygen-fuel thermal spraying on the physical and mechanical properties of type 316 stainless steel. *Journal of thermal spray technology, 14*(3), 369-372.

Tsui, Y. C., & Clyne, T. W. (1997). An analytical model for predicting residual stresses in progressively deposited coatings Part 1: Planar geometry. *Thin Solid Films, 306*(1), 23-33. doi: http://dx.doi.org/10.1016/S0040-6090(97)00199-5

Wenzelburger, M., Escribano, M., & Gadow, R. (2004). Modeling of thermally sprayed coatings on light metal substrates: – layer growth and residual stress formation. *Surface and Coatings Technology, 180–181*(0), 429-435. doi: http://dx.doi.org/10.1016/j.surfcoat.2003.10.125

Williamson, R., Rabin, B., & Drake, J. (1993). Finite element analysis of thermal residual stresses at graded ceramic-metal interfaces. Part I. Model description and geometrical effects. *Journal of Applied Physics, 74*(2), 1310-1320.

Yokoyama, K., Watanabe, M., Kuroda, S., Gotoh, Y., Schmidt, T., & Gartner, F. (2006). Simulation of solid particle impact behavior for spray processes. *Materials transactions, 47*(7), 1697.

Zhang, X., Watanabe, M., & Kuroda, S. (2013). Effects of residual stress on the mechanical properties of plasma-sprayed thermal barrier coatings. *Engineering Fracture Mechanics, 110*(0), 314-327. doi: http://dx.doi.org/10.1016/j.engfracmech.2013.08.016

Zhang, X. C., Xu, B. S., Wang, H. D., Jiang, Y., & Wu, Y. X. (2006). Modeling of thermal residual stresses in multilayer coatings with graded properties and compositions. *Thin Solid Films, 497*(1–2), 223-231. doi: http://dx.doi.org/10.1016/j.tsf.2005.09.184

Zirari, M., Abdellah El-Hadj, A., & Bacha, N. (2010). Numerical analysis of partially molten splat during thermal spray process using the finite element method.

Applied Surface Science, 256(11), 3581-3585. doi: http://dx.doi.org/10.1016/j.apsusc.2009.12.158

Zouari, B., & Touratier, M. (2002). Simulation of organic coating removal by particle impact. *Wear, 253*(3–4), 488-497. doi: http://dx.doi.org/10.1016/S0043-1648(02)00141-2

APPENDIX A: ABAQUS MODEL CODE

The following code contains instructions written in Python Scripting Language to define several models developed in Abaqus FEA. These models should be run in Abaqus CAE, employing the Run Script option. With the exception of the implicit iterative model, the rest of models will wait for the user

command before performing any analysis. For practical purposes, the whole code is not included in the physical format of this thesis. Only the script name is specified for the following models and the reader should be referenced to the digital version of this thesis, which includes adequate Python scripts. The models should be computed in the following order.

Layer-by-Layer Heat Transfer Uncoupled Model:

Script name: layer_heat_transfer.py

Layer-by-Layer Thermal Stress Uncoupled Model:

Script name: layer_thermal_stress.py

Explicit-Implicit Residual Stress Iterative Implementation:

Script name: implicit_iterative.py

Layer-by-Layer Peening Stress Uncoupled Model:

Script name: layer_peening_stress.py